Mechanistic and Functional Studies of the Interaction of a Proline-rich Antimicrobial Peptide with Mammalian Cells*

Linda Tomasinsig[‡§], **Barbara Skerlavaj**[‡], **Niv Papo**[¶], **Barbara Giabbai**[‡1], **Yechiel Shai**[¶], and **Margherita Zanetti**[‡§2]

From the ‡Department of Biomedical Sciences and Technology, University of Udine, P.le Kolbe 4, I-33100 Udine, Italy, §National Laboratory Interuniversity Consortium for Biotechnology, Area Science Park, Padriciano 99, I-34012 Trieste, Italy, and ¶Department of Biological Chemistry, The Weizmann Institute of Science, Rehovot 76100, Israel

Mammalian antimicrobial peptides provide rapid defense against infection by inactivating pathogens and by influencing the functions of cells involved in defense responses. Although the direct antibacterial properties of these peptides have been widely characterized, their multiple effects on host cells are only beginning to surface. Here we investigated the mechanistic and functional aspects of the interaction of the proline-rich antimicrobial peptide Bac7(1–35) with mammalian cells, as compared with a truncated analog, Bac7(5–35), lacking four critical N-terminal residues (RRIR) of the Bac7(1–35) sequence. By using confocal microscopy and flow cytometry, we showed that although the truncated analog Bac7(5–35) remains on the cell surface, Bac7(1–35) is rapidly taken up into 3T3 and U937 cells through a nontoxic energy- and temperature-dependent process. Cell biology-based assays using selective endocytosis inhibitors and spectroscopic and surface plasmon resonance studies of the interaction of Bac7(1–35) with phosphatidylcholine/cholesterol model membranes collectively suggest the concurrent contribution of macropinocytosis and direct membrane translocation. Structural studies with model membranes indicated that membrane-bound Bac7(5–35) is significantly more aggregated than Bac7(1–35) due to the absence of the N-terminal cationic cluster, thus providing an explanation for hampered cellular internalization of the truncated form. Further investigations aimed to reveal functional implications of intracellular uptake of Bac7(1–35) demonstrated that it correlates with enhanced S phase entry of 3T3 cells, indicating a novel function for this proline-rich peptide.

An impressive array of antimicrobial peptides (AMPs)[3] is produced by the inflammatory and epithelial cells of mammals as part of the host response to microbial invasion (1, 2). These molecules all exhibit a net positive charge at neutral pH and an overall amphipathic topology that favors their binding to and insertion into anionic phospholipids, leading to rapid disruption of the bacterial membranes (2, 3). AMPs efficiently kill a variety of microbial pathogens both *in vitro* and *in vivo* (2, 4), and some of them have been shown to also modulate various cellular responses (5, 6). The latter finding has led to a re-evaluation of the role of AMPs in immunity, suggesting their involvement in recruitment, activation, and/or maturation of inflammatory and immune cells and/or tissue repair (5, 6). The multiple activities of AMPs underscore their capacity to interact with host cells by binding to cell surface receptor(s), as exemplified by binding of the α-helical peptide LL-37 to the formyl peptide receptor-like 1 (7), or by binding intracellular targets, as indicated by the ability of the proline-rich cathelicidin peptide PR-39 to interact with various cytoplasmic proteins (8–10).

Among the mammalian AMPs, PR-39 and other proline-rich cathelicidin AMPs, such as the 59-residue Bac7 and the Bac7(1–35) fragment, are peculiar because they kill bacteria without inducing gross destabilization of the bacterial membranes (11). In addition to affecting bacterial viability, PR-39 also appears to do the following: up-regulate the expression of cell surface proteoglycans that are required for cellular responses to heparin-binding growth factors and extracellular matrix components (12); induce chemotaxis of neutrophils (13); promote angiogenesis (14); and inhibit hypoxia-induced apoptosis in vascular endothelial cells (15). The pleiotropic effects of this peptide suggest it may protect the host by influencing selected cellular functions in connection with specific pathophysiological settings.

Despite a wealth of information on the effects of PR-39 on host cells, little is known about the role(s) of other proline-rich AMPs besides their direct antimicrobial activity. We addressed this issue and explored the cell interaction properties of Bac7(1–35) to increase our understanding of the mechanisms of peptide-cell interaction and their functional implications in mediating the diverse roles of AMPs in immunity, and how these peptides globally impact on host defense. This information is vital to the potential development of these peptides or derivatives as therapeutic molecules.

The sequence of Bac7(1–35) (16 prolines out of 35 amino acid residues) comprises an N-terminal cationic cluster (RRIR) followed by regular Pro/Arg repeats interrupted by highly hydrophobic residues. Bac7(1–35) has been shown to kill Gram-negative bacteria (16) and to evoke selected transcriptional responses in *Escherichia coli* (17). Previous structure/activity relationship studies of this peptide demonstrated that removal of the N-terminal (RRIR) residues from the sequence of Bac7(1–35) dramatically reduced (16) or abolished (17) these effects.

Here we investigated the potential of Bac7(1–35) to interact with cultured mammalian cells and to affect cellular functions. The truncated analog Bac7(5–35) lacking the 1–4 N-terminal residues was examined in parallel to determine the role of the cationic N-terminal cluster in this interaction. By using three independent methods, *i.e.* confocal microscopy, flow cytometry, and quantitative spectrofluorometric measurements of cells treated with fluorescein-labeled peptides,

[3] The abbreviations used are: AMP, cationic antimicrobial peptide; ATR-FTIR, attenuated total reflection-Fourier transform infrared spectroscopy; SPR, surface plasmon resonance; PC, egg phosphatidylcholine; FM 4-64, *N*-(3-triethylammoniopropyl)-4-(6-(4-(diethylamino)phenyl)hexatrienyl)pyridinium dibromide); diS-C$_3$-5, 3,3′-diethylthiodicarbocyanine iodide; MIC, minimum inhibitory concentration; Fmoc, *N*-(9-fluorenyl)methoxycarbonyl; DMEM, Dulbecco's modified Eagle's medium; FCS, fetal calf serum; BrdUrd, bromodeoxyuridine; LDH, lactate dehydrogenase; MCD, methyl-β-cyclodextrin; SUV, small unilamellar vesicle; RU, response unit; PBS, phosphate-buffered saline.

we found that although the N-terminally truncated analog Bac7(5–35) accumulated on the cell surface and was poorly internalized, Bac7(1–35) was rapidly taken up by cells and was localized to the cytoplasm and nucleus. The use of various drugs that affect endocytic pathways suggested the involvement of macropinocytosis in the internalization process. Further studies of the membrane interaction properties of the two peptides using ATR-FTIR spectroscopy and SPR with model PC/cholesterol membranes provided a physical explanation for the poor cellular incorporation of Bac7(5–35) and revealed a strong tendency of Bac7(1–35) to insert into lipid membranes, suggesting the concurrence of direct membrane translocation besides macropinocytosis. Finally, functional implications of intracellular Bac7(1–35) were inferred from the ability of Bac7(1–35), but not Bac7(5–35), to enhance S phase entry in fibroblasts.

EXPERIMENTAL PROCEDURES

Materials—Derivatized PEG-PS resins, coupling reagents for peptide synthesis, and Fmoc amino acids were from Applied Biosystems (Foster City) and ChemImpex (Wood Dale, IL). All other reagents and solvents were of synthesis grade. Lucifer yellow, 5(and 6-)-carboxyfluorescein succinimidyl ester (mixed isomers), *N*-(3-triethylammoniopropyl)-4-(6-(4-(diethylamino)phenyl)hexatrienyl)pyridinium dibromide (FM 4-64), and 3,3′-diethylthiodicarbocyanine iodide (diS-C$_3$-5) were from Molecular Probes (Leiden, The Netherlands). All other reagents were of analytical grade.

Peptide Synthesis and Fluorescein Labeling—Bac7(1–35) (RRIRPRPPRLPRPRPRPRPLPFPRPGPRPIPRPLPFP), Bac7(5–35) (PRPPRLPRPRPRPLPFPRPGPRPIPRPLPFP), and LL-37 (LLGDFFRKSKEKIGKEFKRIVQRIKDFLRNLVPRTES) were chemically synthesized by Fmoc solid phase peptide synthesis on a Milligen 9050 automated synthesizer (Applied Biosystems, Foster City) (18). The difficult coupling steps predicted in the synthesis of LL-37 were carried out as described (19). An extra lysine residue was added at the C terminus of Bac7(1–35) and Bac7(5–35) to attach the fluorescein moiety. Fluorescein labeling was conducted according to Rapaport and Shai (20). The completion of the reaction was monitored by the ninhydrin assay (21). After removal of the N-terminal Fmoc protection, peptides were cleaved from the resin and purified by high pressure liquid chromatography as reported previously (18, 19). The identity of the peptides was confirmed by electrospray mass spectrometry, using an API I instrument (PerkinElmer Life Sciences). The concentration of fluorescein-conjugated peptides was determined by measuring the fluorescein absorbance at 495 nm and using an extinction coefficient of 74,000 according to the manufacturer. The concentration of unlabeled peptides was determined by measuring the absorbance of Phe residues at 257 nm as described previously (18).

Antibacterial Assay—The *in vitro* antibacterial activity was determined as the minimum inhibitory concentration (MIC) by a microdilution susceptibility test in 96-well microtiter plates, according to the guidelines of the National Committee for Clinical Laboratory Standards. The activity was measured in Mueller-Hinton broth (Difco) using logarithmic phase microorganisms as reported previously (22).

Cells and Cell Cultures—NIH 3T3 murine fibroblastic cells were cultured under 5% CO$_2$ at 37 °C as exponentially growing subconfluent monolayers in Dulbecco's modified Eagle's medium (DMEM) supplemented with 10% (v/v) fetal calf serum (FCS) and 2 mM glutamine. U937 human monocytic cells were cultured in suspension in RPMI 1640 medium supplemented with 10% (v/v) FCS and 2 mM glutamine.

DNA Synthesis Assay—NIH 3T3 cells (1×10^4/cm^2) were seeded on coverslips (Nunc Inc.) in 35-mm-diameter dishes and incubated at 37 °C in complete DMEM. After 24 h, the cell culture medium was

replaced with DMEM containing 0.5% FCS, and the incubation was prolonged for 48 h. After this time, addition of 50 μM bromodeoxyuridine (BrdUrd) for 60 min resulted in less than 5% of BrdUrd-positive nuclei. Growth-arrested cells were incubated in DMEM containing 2% FCS and 50 μM BrdUrd, in the absence or presence of the selected peptide. After 18 h cells were fixed with 4% paraformaldehyde in PBS and processed for immunofluorescence as described (23). DNA synthesis was assessed by counts of BrdUrd-positive cell nuclei over total cell nuclei after BrdUrd incorporation.

Confocal Laser Microscopy—NIH 3T3 cells were seeded on coverslips or on glass bottom dishes (WillCo Wells BV) and incubated overnight at 37 °C in complete DMEM. The cell culture medium was then replaced with Opti-MEM (Invitrogen) containing 5 μM fluorescein-labeled peptide, with or without 10 μM FM 4-64, and incubation continued for the appropriate time. U937 cells were grown at 37 °C in complete RPMI 1640, incubated for the appropriate times at 1.6×10^6 cells/ml with Opti-MEM containing 5 μM fluorescein-labeled peptide, washed, and transferred to slides by cytocentrifugation. After washing with Opti-MEM, cells were either examined directly by confocal microscopy or fixed with 4% paraformaldehyde in PBS at room temperature for 20 min or with acetone/methanol (1:1) at 4 °C for 3 min. After fixation, cells were mounted on coverslips for fluorescence microscopic examination. Data were obtained using a Leica TCS laser scan microscope equipped with 488 nm argon ion laser and with 543 nm helium-neon ions laser. Optical sections collected at different levels perpendicular to the optical axis are presented. Photomultiplier gain and laser power were identical within each experiment.

Flow Cytometry—Cells were incubated in Opti-MEM in the presence of 5 μM fluorescein-tagged Bac7(1–35) or 4 μM fluorescein-tagged LL-37 at 37 °C for 60 min, washed twice with PBS, and treated with 1 mg/ml trypsin at 37 °C for 5 min to remove surface-bound peptide. This treatment did not affect cell viability, as determined by the trypan blue exclusion assay, while effectively reducing the fluorescein signal, as indicated by fluorescence-activated cell sorter analysis in the absence and presence of trypsin treatment. Cells were then washed and resuspended in PBS for analysis. For energy depletion studies, cells were preincubated at 37 °C for 30 min in Opti-MEM containing 10 μM oligomycin B and 50 mM 2-deoxy-D-glucose before incubation with the peptide at 37 °C for 60 min in the same medium. This procedure resulted in a 90–95% reduction in the cellular ATP pool as determined by using the luciferin-luciferase assay kit from Molecular Probes. The viability of ATP-depleted cells as determined by the trypan blue exclusion assay was never lower than 93%. To study the effect of low temperature, cells were pre-cooled at 4 °C for 30 min and then incubated with the peptide at 4 °C for 60 min in the same medium. To address the effect of endocytosis inhibitors, cells were preincubated for 60 min at 37 °C with 10 mM methyl-β-cyclodextrin (MCD) or 10 mM amiloride or 0.1 mM cytochalasin D or 20 μM nocodazole. Cells were then incubated with the peptide in the presence of each drug for 60 min. Samples were analyzed with a flow cytometer equipped with the Cell Quest software by using a 488-nm argon ion laser (FACScan, BD Biosciences). A minimum of 10,000 events per sample was analyzed.

Fluorescence Quantification—U937 cells (5×10^6/ml) were incubated with 5 μM fluorescein-tagged peptide in Opti-MEM at 37 °C for 10, 30 and 60 min, washed twice with the same solution and once with PBS, incubated with trypsin at 1 mg/ml for 5 min at 37 °C, washed with PBS, resuspended in the same buffer, and processed by sonication for fluorescence measurements. To obtain the cytoplasmic and nuclear fractions, cells were subjected to hypotonic lysis by a 45-min swelling in hypotonic buffer (10 mM Hepes, pH 7.9, 1.5 mM MgCl$_2$, 10 mM KCl, 0.2

mM phenylmethanesulfonyl fluoride, 0.5 mM dithiothreitol, and 10 μg/ml each of chymostatin, leupeptin, antipain and pepstatin A) on ice, followed by three freeze-thaw cycles. Nuclei were separated from the cytoplasmic fraction by centrifugation at 1,000 × g for 10 min, washed once, and resuspended in PBS. The cytoplasmic extract was added with 1:10 v/v cytoplasmic extract buffer (0.3 M Hepes, pH 7.9, 1.4 M KCl, 0.03 M MgCl$_2$, 0.2 mM phenylmethanesulfonyl fluoride, 0.5 mM dithiothreitol, and 10 μg/ml each of chymostatin, leupeptin, antipain, and pepstatin A). Fluorescence was quantified in duplicate with excitation set at 488 nm, emission at 525 nm, and cut off at 515 nm. Protein was measured with the Bradford reagent (Bio-Rad). Results are expressed as picomoles of peptide/mg of cellular protein.

Cytotoxicity—Cells were incubated for 60 min at 37 °C in Opti-MEM in the absence or presence of each peptide. The LDH activity of cell-free media and cell lysates (obtained by treating cell pellets for 5 min with 0.1% Triton X-100) was determined by measuring the decrease in the absorbance of NADH at 340 nm (24). LDH activity in the culture media was expressed as percent of total cellular LDH activity.

Membrane Permeability Assay on Small Unilamellar Vesicles (SUVs)—SUVs were prepared by sonication of PC/cholesterol (10:1, w/w) dispersions as described previously (25). Vesicles were unilamellar with an average diameter of 20–50 nm, as confirmed by electron microscopy (JEOL JEM 100B instrument, Japan Electron Optics Laboratory Co., Tokyo, Japan). Peptide-induced membrane destabilization of SUVs, which results in the collapse of the diffusion potential, was detected as an increase in fluorescence of the potential sensitive dye diS-C$_3$-5 (26–28).

ATR-FTIR Measurements and Data Analysis—Spectra were obtained with a Bruker Equinox 55 FTIR spectrometer equipped with a deuterated triglyceride sulfate detector and coupled to an ATR device as described in detail previously (29). Briefly, a mixture of lipids (0.5 mg) alone or with peptide (~20 μg) was deposited on a ZnSe horizontal ATR prism (80 × 7 mm). Prior to sample preparation, the trifluoroacetate counterions were replaced with chloride ions to eliminate an absorption band near 1673 cm^{-1} (30). Lipid/peptide mixtures were prepared by dissolving them together in a 1:2 CH$_3$OH/CH$_2$Cl$_2$ mixture and drying under a stream of dry nitrogen. Spectra were recorded, and the respective pure phospholipid spectra were subtracted to yield the difference spectra. Hydration of the sample was achieved by incubating in D$_2$O for 2 h before acquisition of the spectra. H/D exchange was considered complete after a total shift of the amide II band. Prior to curve fitting, a straight base line passing through the ordinates at 1700 and 1600 cm^{-1} was subtracted. The spectra were processed using PEAK-FIT^{TM} software (Jandel Scientific, San Rafael, CA). Second-derivative spectra accompanied by 13-data point Savitsky-Golay smoothing were calculated to identify the positions of the component bands in the spectra. These wave numbers were used as initial parameters for curve fitting with gaussian component peaks. Position, bandwidths, and amplitudes of the peaks were varied as follows: (i) until the resulting bands shifted by no more than 2 cm^{-1} from the initial parameters; (ii) until all the peaks had reasonable half-widths (<20–25 cm^{-1}), and (iii) until good agreement between the calculated sum of all the components and the experimental spectra was achieved (r^2 >0.99). The relative contents of different secondary structure elements were estimated by dividing the areas of individual peaks, assigned to a specific secondary structure, by the whole area of the resulting amide I band. The results of four independent experiments were averaged. The ATR electric fields of incident light were calculated as described previously (31, 32). Lipid order parameters were obtained from the symmetric (ν_{sym}(CH$_2$) ~2853 cm^{-1}) and the antisymmetric ($\nu_{antisym}$(CH$_2$) ~2922 cm^{-1}) lipid stretching mode (32).

Binding Analysis by Surface Plasmon Resonance Biosensor—Biosensor experiments were carried out with a BIAcore 3000 analytical system (Biacore, Uppsala, Sweden) using L1 sensor chip (BIAcore), which allows the formation of a lipid bilayer (33). All solutions were freshly prepared, degassed, and filtered through 0.22-μm pores. Experiments were done at 25 °C. After cleaning the chip by an injection of 40 mM *N*-octyl-β-D-glucopyranoside (25 μl), at a flow rate of 5 μl/min, PC/cholesterol (10:1 w/w) SUVs (80 μl, 0.5 mM) were applied to the chip surface at a low flow rate of 2 μl/min, which then was increased to 50 μl/min, resulting in a stable base line. Bovine serum albumin was then injected (25 μl, 0.1 mg/μl in PBS) to cover nonspecific binding sites. Peptide solutions (a 50-μl PBS solution of 0.78–100 μM peptide) were injected on the lipid surface at a flow rate of 5 μl/min. PBS alone was then replaced by the peptide solution for 30 min to allow peptide dissociation. SPR detects changes in the reflective index of the surface layer of peptides and lipids in contact with the sensor chip. A sensogram was obtained by plotting the SPR angle against time. The peptide-lipid binding event was analyzed from a series of sensograms collected at seven different peptide concentrations.

The sensograms for each peptide-lipid bilayer interaction (L1 chip) were analyzed by curve fitting using numerical integration analysis (34). The BIAevaluation software offers different reaction models to perform complete kinetic analyses of the peptide sensograms. One curve-fitting algorithm (the two-state reaction model) was chosen on the basis of what was known about the possible binding mechanisms of lytic peptides. The data were fitted globally by simultaneously fitting the peptide sensograms obtained at seven different concentrations. The two-state reaction model was applied to each data set. This model describes two reaction steps (33) which, in terms of peptide-lipid interaction, corresponds to Reaction 1,

$$P + L \underset{k_{d1}}{\overset{k_{a1}}{\rightleftharpoons}} PL \underset{k_{d2}}{\overset{k_{a2}}{\rightleftharpoons}} PL^*$$

REACTION 1
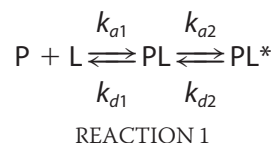
where in the first step, peptide (P) binds to lipids (L) to give PL, which is changed to PL* in the second step. PL* cannot dissociate directly to P + L and may correspond to partial insertion of the peptide into the lipid bilayers. The corresponding differential rate equations for this reaction model are represented by Equations 1 and 2,

$$dRU_1/dt = k_{a1} \times C_A \times (RU_{max} - RU_1 - RU_2)$$
$$- k_{d1} \times RU_1 - k_{a2} \times RU_1 + k_{d2} \times RU_2 \quad \text{(Eq. 1)}$$

$$dRU_2/dt = k_{a2} \times RU_1 - k_{d2} \times RU_2 \quad \text{(Eq. 2)}$$

where RU$_1$ and RU$_2$ are the response units for the first and second steps, respectively; C_A is the peptide concentration; RU$_{max}$ is the maximal response unit (or equilibrium binding response); and k_{a1}, k_{d1}, k_{a2}, and k_{d2} are the association and dissociation rate constants for the first and second steps, respectively. Whereas k_a has 1/(M× s) units, k_{d1}, k_{d2}, and k_{a2} have 1/s units. Thus the total affinity constant for the all process, K, has M^{-1} units.

RESULTS

Antimicrobial Activity—The antimicrobial activities of the compounds under study were examined to rule out functional modifications

induced by fluorescein conjugation. No substantial changes were observed when comparing the activities of labeled *versus* unlabeled peptides toward *E. coli* ATCC 25922 and *Staphylococcus aureus* ATCC 25923 (Table 1). Bac7(5–35) was found to exhibit 64-fold higher MIC compared with Bac7(1–35) against *E. coli* ATCC 25922, and both Bac7(1–35) and Bac7(5–35) were inactive toward *S. aureus* ATCC 25923 up to 32 μM, in good agreement with the data obtained with these peptides in prior assays (16). The human cathelicidin LL-37 was used in this study as a paradigm of α-helical membranolytic peptide (35, 36). The MIC values of fluorescein-labeled LL-37 against both bacterial strains compared favorably with those of the unlabeled peptide (Table 1) and are in line with prior studies (37).

Internalization Efficiency and Intracellular Localization—To investigate their potential to enter mammalian cells, each fluorescein-tagged peptide was added at a concentration of 5 μM to cultures of murine NIH 3T3 fibroblastic and human U937 monocytic cell lines, which were then examined by confocal laser scanning microscopy. Bac7(1–35) was detected in the cytoplasm as well as in the nuclei, both in formaldehyde-

TABLE 1
Antimicrobial activity of peptides used in this study
MIC was defined as the lowest concentration of peptide that prevented visible growth of *E. coli* ATCC 25922 or *S. aureus* ATCC 25923 after incubation for 18 h at 37 °C. Results are the mean of at least four independent experiments.

Peptide	MIC	
	E. coli ATCC 25922	*S. aureus* ATCC 25923
	μM	
Bac7(1–35)	0.25	>16
Bac7(1–35)[a]	0.5	>16
Bac7(5–35)	16	>32
Bac7(5–35)[a]	16	>32
LL-37	8	>32
LL-37[a]	8	>32

[a] This is a fluorescein-labeled peptide.

(Fig. 1, *A* and *C*) and methanol/acetone-fixed cells (not shown). Microscopic examinations of live unfixed 3T3 cells after removal of the peptide solution confirmed this cellular distribution (Fig. 1B). To examine the fluorescence pattern associated with the truncated analog Bac7(5–35), a *z*-series was taken through 3T3 cells co-incubated with Bac7(5–35) and the styryl dye FM 4-64 (two representative sections collected at different levels are shown in Fig. 1, *D–I*). Bac7(5–35) was only detected at the cell surface (Fig. 1D), whereas the red fluorescence associated with FM 4-64 was also present in lower sections (compare *E* and *H* in Fig. 1), in accord with the reported ability of this dye to emit intense red fluorescence when inserted into lipid membranes and in membrane-derived endocytic vesicles (38, 39).

The kinetics of the internalization process assessed by spectrofluorometric measurements of total cell extracts indicated that Bac7(1–35) was rapidly internalized in U937 cells during the first 30 min (Fig. 2A), whereas cells incubated with Bac7(5–35) revealed a markedly reduced signal at all time points considered (Fig. 2A). The low rate of incorporation of Bac7(5–35) was confirmed by separate assessments of the fluorescence associated with nuclear and cytoplasmic extracts after a 30-min incubation with either peptide (Fig. 2B) and by flow cytometry of U937 cells treated with each peptide for 30 min. By using the latter technique, the intracellular fluorescein signal derived from Bac7(5–35) was never higher than 10% that recorded with Bac7(1–35) (data not shown).

Cytotoxicity—Potential lytic effects associated with cell entry were assessed by measuring the activity of the cytoplasmic enzyme LDH in the culture medium of peptide-treated cells. The LDH activity was negligible after 60 min of incubation with fluorescein-tagged Bac7(1–35) (Table 2) and was never higher than 1.5% in the presence of unlabeled Bac7(1–35) up to 50 μM (not shown), indicating that the incorporation of Bac7(1–35) was not accompanied by significant membrane pertur-

FIGURE 1. **Localization of Bac7(1–35) and Bac7(5–35) in NIH 3T3 (*A, B, and D–I*) and U937 (*C*) cells.** NIH 3T3 (*A*) and U937 (*C*) cells were treated for 30 min with 5 μM fluorescein-conjugated Bac7(1–35) and observed by confocal laser fluorescence microscopy after fixation with paraformaldehyde. NIH 3T3 cells were incubated with 5 μM fluorescein-conjugated Bac7(1–35) for 30 min and observed unfixed by confocal microscopy (*B*). NIH 3T3 cells were co-incubated for 30 min with 5 μM fluorescein-tagged Bac7(5–35) (*D* and *G*) and 10 μM FM 4-64 (*E* and *H*) and observed without fixation. Image merging of Bac7(5–35) and FM 4-64 is shown in *F* and *I*. Section represented in *G–I* was collected at 1.62-μm interval along the *z*-axis from the section represented in *D–F*. Magnification ×63.
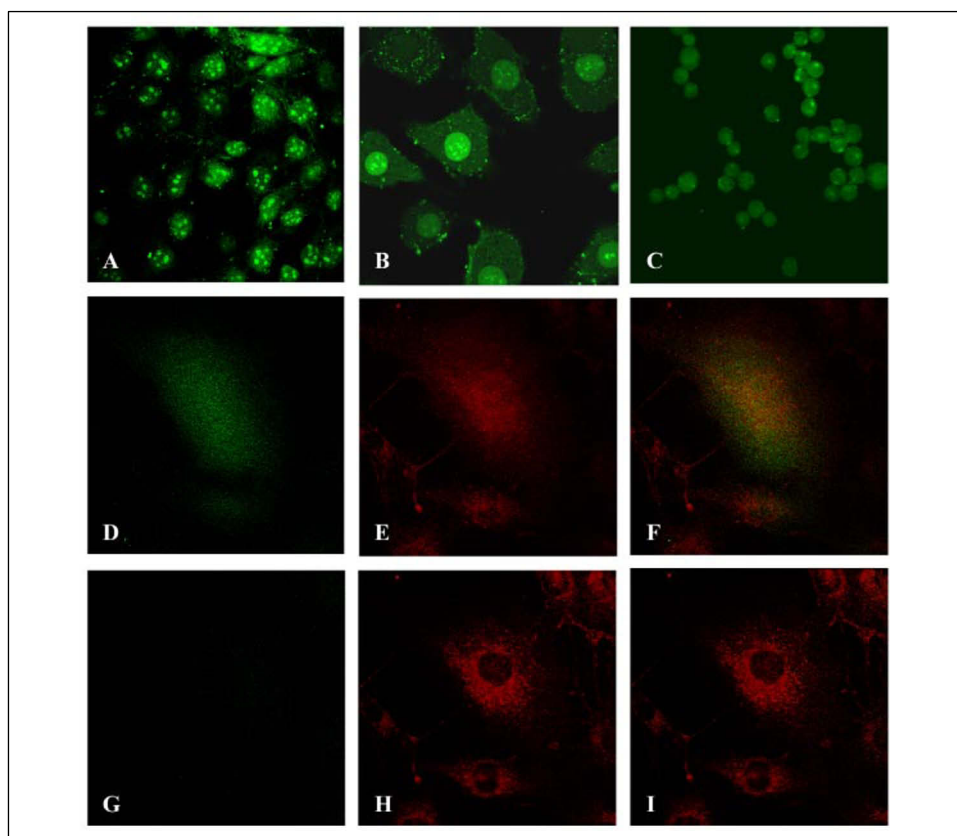
FIGURE 2. **Kinetics of cellular internalization (*A*) and cytoplasmic and nuclear incorporation (*B*) of Bac7(1–35) and Bac7(5–35) in U937 cells.** *A,* cells were incubated with 5 μM fluorescein-tagged Bac7(1–35) (*diamonds*) or with 5 μM fluorescein-tagged Bac7(5–35) (*circles*) at 37 °C for the indicated times. After incubation, cells were washed thoroughly and lysed by ultrasonication. *B,* cells were incubated with fluorescein-tagged Bac7(1–35) (*open bars*) or with fluorescein-tagged Bac7(5–35) (*black bars*) at 37 °C for 30 min and then washed, and the cytoplasmic and nuclear fractions were separated as described under "Experimental Procedures." Fluorescence was measured using a SpectraMax Gemini XS fluorescence spectrophotometer. Data represent the mean ± S.D. of at least three independent experiments.
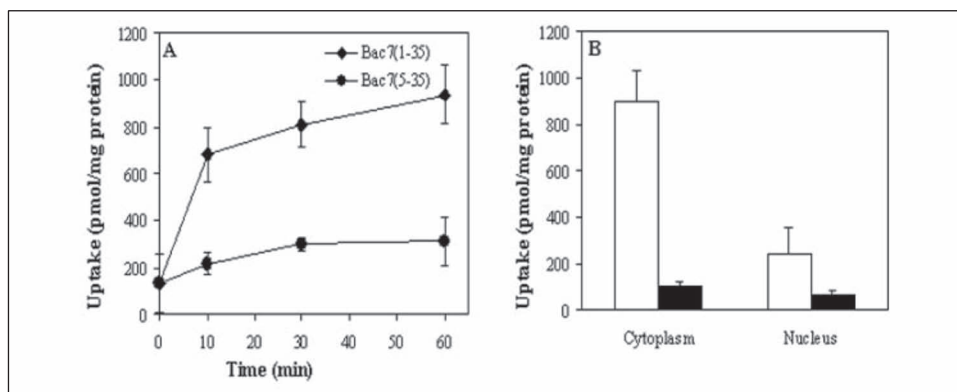

TABLE 2

LDH activity released in the supernatant of peptide-treated cells

LDH activity was measured in the supernatant of U937 or 3T3 cells incubated at 37 °C for 60 min in the presence of each peptide. The activity released in the extracellular medium is expressed as percentage of total cellular LDH activity after subtraction of the activity released from untreated cells (1.2 ± 0.3%). Data are mean ± S.D. of at least four independent experiments.

	U937	NIH3T3
	%	
Bac7(1–35) 5 μM	0.3 ± 0.02	0.4 ± 0.01
Bac7(1–35) 50 μM	1.1 ± 0.05	1.5 ± 0.04
LL-37 10 μM	38.0 ± 3.1	38.0 ± 2.7

bation. By comparison, incubation of cells with 10 μM LL-37 resulted in marked increase of the extracellular LDH activity (Table 2), confirming the membranolytic activities of LL-37 at this peptide concentration (36).

Effects of Metabolic Inhibitors, Low Temperature, and Endocytosis Inhibitors—To assess whether the internalization of extracellular Bac7(1–35) required metabolic cellular processes, we examined the incorporation of Bac7(1–35) in metabolically active *versus* energy-depleted cells by flow cytometry. Additionally, the temperature dependence of this process and the effect of endocytosis inhibitors were investigated.

A marked decrease in the fluorescein signal was observed by analysis of both ATP-depleted and low temperature cells exposed to Bac7(1–35) for 60 min (Fig. 3*A*), consistent with involvement of an active uptake mechanism. The role of endocytic pathways was examined by incubating cells for 60 min in the presence of pharmacological inhibitors of cellular processes associated with endocytosis, prior to addition of Bac7(1–35). The contribution of macropinocytosis was assessed by pretreating cells with amiloride, a sodium/proton pump inhibitor that impairs macropinocytosis (40) with little effect on caveolae- or clathrin-based endocytosis (41). Incubation of cells with 10 mM amiloride reduced the internalization of Bac7(1–35) by 70 and 40% respectively, in U937 and 3T3 cells (Fig. 3*A*). The influence of cytochalasin D, which induces depolymerization of actin filaments, was examined in view of the contribution of actin in the formation of macropinosomes (42). Cell treatment with this compound at 100 μM also decreased the incorporation of Bac7(1–35) by 70% in U937 and by 40% in 3T3 cells. The incorporation into U937 was also inhibited by MCD, which sequesters membrane cholesterol, suggesting the involvement of lipid-raft-dependent macropinocytosis. This drug, however, did not affect the internalization into 3T3 cells (Fig. 3*A*). Finally, 20 μM nocodazole, a microtubule-disrupting drug, reduced uptake by 50% in U937 cells and by 30% in 3T3 cells (Fig. 3*A*).

We examined in parallel the effect of these drugs on LL-37 uptake by U937 cells at a nonlytic (4 μM) peptide concentration, as determined by
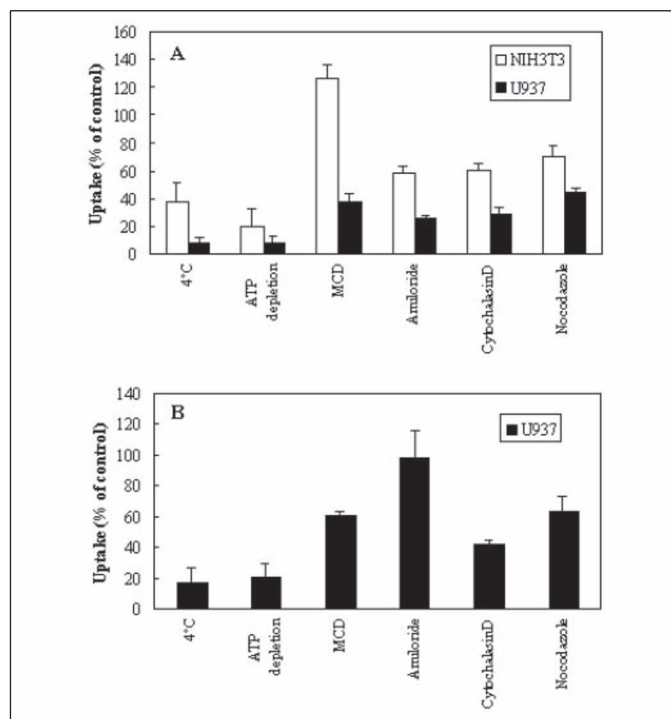

FIGURE 3. **Influence of ATP depletion, low temperature, and endocytosis inhibitors on the cellular uptake of Bac7(1–35) (*A*) and LL-37 (*B*).** U937 and 3T3 cells were either energy-depleted by a 30-min treatment at 37 °C with 10 μM oligomycin B and 50 mM 2-deoxy-D-glucose or were preincubated at 4 °C for 30 min, or pretreated for 60 min at 37 °C with the indicated inhibitors, prior to addition of 5 μM Bac7(1–35) (*A*) or 4 μM LL-37 (*B*). Incubations in the presence of fluorescein-tagged peptides were prolonged for 60 min. Cells were then treated with trypsin to remove membrane-bound peptide, washed in ice-cold PBS, and analyzed by flow cytometry. Uptake of the fluorescein-labeled peptides was quantified as the mean fluorescence intensity and expressed as a percentage of peptide uptake in control cells. Each point is the mean ± S.D. of at least four independent experiments.

measuring LDH release from treated U937 cells (not shown). LL-37 was used because this peptide is taken up into epithelial cells through a process that requires functional endocytic pathways (43). Flow cytometry data using U937 cells and LL-37 supported the contribution of membrane cholesterol and excluded involvement of macropinocytosis based on uptake inhibition by MCD but not amiloride (Fig. 3*B*).

Dissipation of Diffusion Potential Assay—Dissipation of diffusion potential experiments were performed to test whether Bac7(1–35) and Bac7(5–35) were able to increase the permeability of SUVs composed of phospholipids that mimic the composition of mammalian cell membranes. Neither peptide caused an increase in the permeability of PC/cholesterol membranes (Fig. 4) compared with the active control,
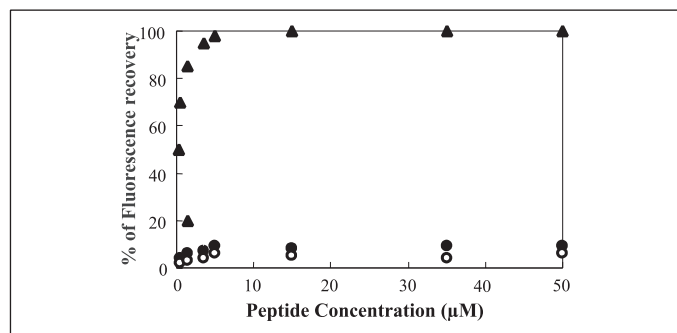
FIGURE 4. **Maximal dissipation of the diffusion potential in PC/cholesterol vesicles, as a function of peptide concentration.** Bac7(1–35) (●), Bac7(5–35) (○), and melittin (▲) were added to PC/cholesterol vesicles pre-equilibrated with the fluorescent dye diS-C$_3$-5 and valinomycin in isotonic K$^+$-free buffer. Fluorescence recovery was measured 3–10 min after the peptides were mixed with the vesicles.
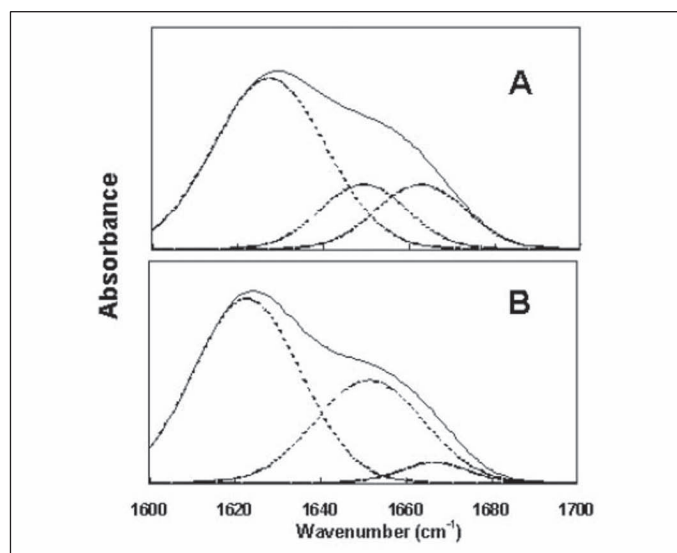

FIGURE 5. **FTIR spectra deconvolution of the fully deuterated amide I band (1600–1700 cm^{-1}) of Bac7(1–35) (*A*) and Bac7(5–35) (*B*) in PC/cholesterol (10:1 w/w) multibilayers.** The component peaks are the result of curve fitting using a gaussian line shape. The sums of the fitted components superimpose on the experimental amide I region spectra. *Bold lines* represent the experimental FTIR spectra after Savitzky-Golay smoothing; *dotted lines* represent the fitted components. A 120:1 lipid/peptide molar ratio was used.

TABLE 3
ATR dichroic analysis of phospholipid multibilayers

Sample[a]	$\nu_{antisymmetric}(CH_2)$	
	R	$R_{L+P} - R_L{}^b$
PC/cholesterol	1.29 (±0.01)	
PC/cholesterol + Bac7(1–35)	1.47 (±0.02)	0.18
PC/cholesterol + Bac7(5–35)	1.37 (±0.01)	0.08
PC/cholesterol + pardaxin[c]	1.46 (±0.02)	0.17
PC/cholesterol + Amphipathic 1D[c]	1.36 (±0.02)	0.07

[a] 1:120 peptide to lipid molar ratio was used.
[b] Designations used are as follows: P indicates peptide; L indicates lipid.
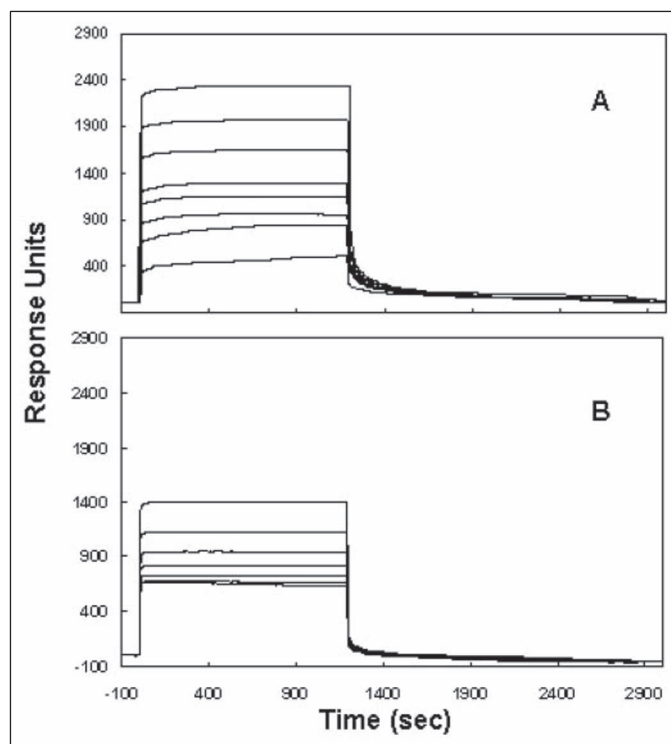[c] Data were taken from Ref. 55.

FIGURE 6. **Sensograms of the binding between various concentrations of Bac7(1–35) (*A*) and Bac7(5–35) (*B*) and the PC/cholesterol (10:1 w/w) lipid bilayer (using L1 chip).** Concentrations used are as follows: 0.78, 1.56, 3.125, 6.25, 12.5, 25, and 50 μM.

the bee venom melittin (44), in good agreement with the absence of cytotoxic effects by these peptides (Table 2).

Secondary Structure of Bac7(1–35) and Bac7(5–35) in Phospholipid Membranes as Determined by FTIR Spectroscopy—The amide I region spectra (*bold lines*) of Bac7(1–35) and Bac7(5–35) bound to PC/cholesterol multibilayers are shown in Fig. 5, *A* and *B*, respectively. Second derivatives are shown for each spectrum as *dotted lines* in Fig. 5, *A* and *B*. The assignment of the different secondary structures to the various amide I regions was calculated according to Refs. 45–51. The assignment to the amide I region between 1620–1625 and 1625–1640 cm^{-1} is characteristic of aggregated β-sheet and β-sheet, respectively. The amide I regions from 1645 to 1655 and from 1656 to 1670 cm^{-1} are characteristic of α-helix and 3$_{10}$-helix, respectively (52). The 3$_{10}$-helical structure for this amide I region was suggested previously in a structural study of phospholipase A$_2$ (53). The analysis of amide I region spectra of membrane-bound peptides indicated a predominant β-sheet structure (63%) for Bac7(1–35) (Fig. 5*A*). Most interestingly, Bac7(5–35) was significantly more aggregated than Bac7(1–35) (Fig. 5*B*) and adopted 61% aggregated β-sheet structure. Because there are no other structural dif-

ferences in the two sequences apart from the 1–4 N-terminal residues (RRIR), the low fraction of aggregated strands found in Bac7(1–35) most likely resulted from repulsion between Bac7(1–35) monomers because of this positively charged cluster.

Orientation of the Phospholipid Membrane and Effect of Bac7(1–35) and Bac7(5–35) on Phospholipid Acyl Chain Order—Polarized ATR-FTIR was used to determine the orientation of the lipid membrane. The symmetric ($\nu_{sym}(CH_2) \sim 2853$ cm^{-1}) and the antisymmetric ($\nu_{antisym}(CH_2) \sim 2922$ cm^{-1}) vibrations of lipid methylene C-H bonds are perpendicular to the molecular axis of a fully extended hydrocarbon chain. Thus, measurements of the dichroism of infrared light absorbance can reveal the order and orientation of the membrane sample relative to the prism surface. The R value based on the stronger $\nu_{antisym}(CH_2)$ of PC/cholesterol (10:1 w/w, 0.5 mg) multibilayers was 1.29 ± 0.01 (Table 3). These data indicate that the phospholipid membrane is well ordered. The observed antisymmetric and symmetric peaks at ~2922 and ~2853 cm^{-1}, respectively, indicated that the membranes were predominantly in a liquid crystalline phase (32, 54), like biological membranes. The effect of Bac7(1–35) and Bac7(5–35) on the multibilayer acyl chains order was estimated by comparing the CH$_2$-

TABLE 4

Association (k_{a1}, k_{a2}) and dissociation (k_{d1}, k_{d2}) rate constants in PC/cholesterol bilayers determined by numerical integration using the two-state reaction model

The affinity constants K_1 and K_2 are for the first ($K_1 = k_{a1}/k_{d1}$) and second ($K_2 = k_{a2}/k_{d2}$) steps, respectively, and the affinity constant (K) determined as (k_{a1}/k_{d1}) × (k_{a2}/k_{d2}) is for the complete binding process. The experiments were repeated three times with an S.D. of 10%.

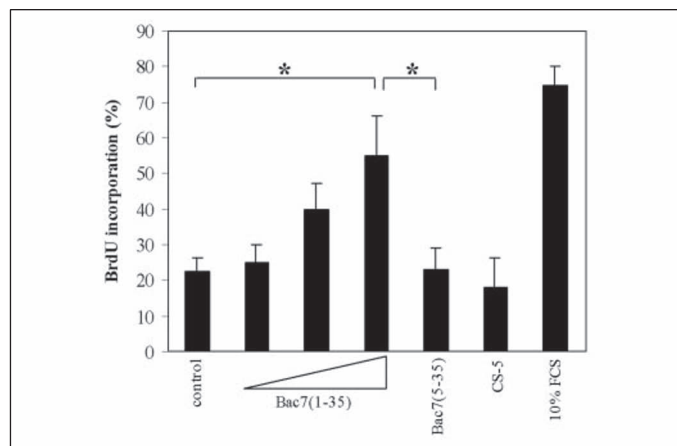| Peptides	k_{a1}	k_{d1}	K_1	k_{a2}	k_{d2}	K_2	K
	$1/\text{M} \times s$	$1/s$	$\times 10^4\ 1/\text{M}$	$1/s$			$\times 10^4\ 1/\text{M}$
Bac7(1–35)	483 (±0.1)	0.005 (±0.0006)	9.6	0.50 (±0.04)	0.003 (±0.0002)	147	1400 (±0.01)
Bac7(5–35)	4580 (±0.9)	0.009 (±0.0001)	50.8	0.03 (±0.01)	0.006 (±0.0003)	5	250 (±0.9)

FIGURE 7. **Induction of DNA synthesis in NIH 3T3 cells treated with Bac7(1–35), Bac7(5–35), or CS-5.** Growth-arrested NIH 3T3 cells were incubated in DMEM containing 2% FCS and 50 μM BrdUrd, in the absence (*control*) and presence of each indicated peptide or in 10% FCS-containing medium. Bac7(1–35) was used at 5, 10, and 20 μM and Bac7(5–35) and CS-5 at 20 μM. The fibronectin fragment denoted CS-5 served as a negative control in these experiments. After 18 h of incubation, cells were fixed and processed for immunofluorescence as described under "Experimental Procedures." Percent BrdUrd incorporation was calculated as the ratio between BrdUrd-positive nuclei and total nuclei. The mean of four experiments $\pm$ S.D. are reported. *, $p < 0.001$.

stretching dichroic ratio of phospholipid multibilayers in the absence or the presence of peptides. The R values are summarized in Table 3. The table also includes two control antimicrobial peptides, *i.e.* amphipathic 1D, which localizes on the surface of the membrane (55), and pardaxin, a peptide that penetrates into the hydrophobic core of PC/cholesterol membranes (55). The increase in the R value ($R_{L+P} - R_L$) in the presence of Bac7(5–35) compared with the lipid alone revealed that incorporation of this peptide did not change significantly the order of the membrane (Table 3), indicating that it was localized near the phospholipid head groups similarly to amphipathic 1D. In contrast, Bac7(1–35) significantly altered the order of the membrane (Table 3), indicating deep insertion into the lipid core (20, 28, 55), similarly to pardaxin. Similar results were obtained when 1:120 or 1:60 peptide-to-lipid molar ratios were used.

Binding Affinity of Bac7(1–35) and Bac7(5–35) to Lipid Bilayers Measured by Surface Plasmon Resonance; a Two-state Model—Typical sensograms of the binding of Bac7(1–35) and Bac7(5–35) with bilayers of PC/cholesterol are shown in Fig. 6, *A* and *B*. Peptide concentrations in the entire assay were similar, thus the RU signals of the peptides could be compared. The sensograms of the binding showed a much higher response level for Bac7(1–35) (Fig. 6*A*) compared with Bac7(5–35) (Fig. 6*B*), indicating higher affinity of the former peptide to these membranes.

We employed numerical integration analysis using a nonlinear method to fit an integrated rate equation directly to the sensograms (33). When fitting the peptides' sensograms globally (using different concentrations of the peptides) with the simplest 1:1 Langmuir binding

model, a poor fit was obtained (data not shown), confirming that this model does not represent the lipid binding mechanism of all the peptides investigated. However, a significantly improved fit was obtained using numerical integration of the two-state reaction model of the binding sensograms. This model reflects a two-step process in the interaction of the peptides with lipid bilayers; the first step is the actual binding, and the second step is the insertion of the peptide into the membrane. A set of peptide sensograms with seven different peptide concentrations was used to estimate the kinetic parameters. The average values for the rate constants obtained from the two-state model analysis are listed in Table 4 along with the affinity constant values (K). The results indicate that the affinity constant, K, determined for Bac7(1–35) was higher than that determined for Bac7(5–35). Furthermore, compared with Bac7(5–35), Bac7(1–35) bound ~15-fold faster (k_{a2}) and dissociated ~2 times slower (k_{d2}) in the second step, resulting in a 30-fold higher insertion constant. In both cases, the second step (K_2, insertion) was slower than the first step (K_1, initial binding).

Effect on DNA Synthesis—Preliminary experiments were performed to investigate the functional capabilities of Bac7(1–35) in relation to its cell interaction properties. We concentrated on the mitogenic potential of this peptide and investigated its ability to enhance the S phase entry of fibroblasts as compared with the truncated analog Bac7(5–35) by measuring the incorporation of BrdUrd into the DNA of NIH 3T3 cells synchronized by growth arrest. Bac7(1–35) was found to induce DNA synthesis in a concentration-dependent manner (Fig. 7). At 20 μM this peptide caused a 2.5-fold induction compared with cells grown in its absence. At the same dose, Bac7(5–35) and a fibronectin fragment denoted CS-5, which was used as a negative control, were ineffective (Fig. 7).

DISCUSSION

In the present study we investigated mechanistic and functional aspects of the interaction of the proline-rich AMP Bac7(1–35) with mammalian cells, by using a cell biology-based approach and biophysical methods using PC/cholesterol membranes. The impetus for this study was the documented ability of other AMPs, including defensins, LL-37 and PR-39, to affect various host cell activities in addition to exerting direct antimicrobial effects (5, 6). Studies of these peptides have revealed significant differences with respect to the mode of peptide-cell interaction (7–10) and functional properties (5) and have stimulated great interest concerning the relevance of their activities in health and disease (2, 56).

We examined fibroblastic (3T3) and monocytic (U937) cells incubated with fluorescein-tagged Bac7(1–35) and obtained evidence that this peptide was efficiently internalized. Confocal images revealed its presence both in the cytoplasm and the nucleus, where it was mostly associated with nucleoli. Artifactual microscopic observations caused by intracellular relocalization of membrane-bound peptide upon cell fixation were ruled out, based on similar patterns of cytoplasmic and nuclear peptide distribution in live and fixed cells. To reduce further the

potential artifacts, membrane-bound but not internalized peptide was removed from cells by a mild trypsin treatment. This enzymatic step effectively reduced the surface fluorescein signal without affecting cell viability.

The role of the 1–4 N-terminal (RRIR) residues of Bac7(1–35) in the peptide-cell interaction was investigated because in prior studies a truncated analog, Bac7(5–35), corresponding to the 5–35-amino acid residues of the Bac7(1–35) sequence, exhibited markedly decreased antibacterial properties (16, 17). In this study we showed that exogenous Bac7(5–35) accumulated on the surface of mammalian cells and was not internalized. To explain this behavior, we performed structural studies in the presence of PC/cholesterol membranes and found that Bac7(5–35) was significantly more aggregated than Bac7(1–35), suggesting that its cellular internalization was hampered by a high propensity to form aggregates on the cell surface. These results support a role for the three extra arginines present in the Bac7(1–35) sequence in lowering the aggregation potential of the monomers by charge repulsion. On these grounds, it is conceivable that the defective antimicrobial activities of Bac7(5–35), as reported previously (16, 17), occurred as a consequence of impaired peptide internalization.

It was important to show that the accumulation of Bac7(1–35) inside cells was not associated with cell lytic activity. We demonstrate here that Bac7(1–35) did not induce release of LDH activity at doses at which a variety of other AMPs are known to cause nonselective membrane permeabilization (4). This result, together with the observation that Bac7(1–35) did not increase the permeability of SUVs that mimic mammalian cell membranes, argues against massive membrane destabilization. A few other AMPs have been shown recently to become incorporated into eukaryotic cells without accompanying toxicity (43, 57–59). For instance, linear derivatives of the disulfide-bonded protegrin appear to accumulate inside K562 cells via adsorption-mediated endocytosis (57), and an endocytic pathway has been implicated in the uptake of LL-37 into A549 cells (43). Conversely, a number of peptide analogs derived from buforin (58), as well as short N-terminal fragments of Bac7(1–24) (59), have been proposed to cross lipid bilayers by direct membrane translocation based, respectively, on transient peptide-lipid pore formation and energy independence of the process. These distinct internalization mechanisms may correspond to functional differences relating to differing localization and/or targets.

Our flow cytometry data indicated that uptake of Bac7(1–35) was energy-dependent and temperature-sensitive, consistent with the contribution of metabolic cellular processes. By exploring further the mechanistic aspects of the uptake process, we found that this was inhibited in U937 cells by MCD and cytochalasin D, suggesting lipid raft- and actin fibers-dependent endocytosis. These results were congruent with the inhibition exerted by amiloride, a specific inhibitor of macropinocytosis (40, 41). In fact, this is a lipid raft-mediated and receptor-independent form of endocytosis requiring actin membrane protrusions to generate endocytic vesicles (42). Overall, our data converge on macropinocytosis being a major uptake mechanism for Bac7(1–35). We further noted that the α-helical peptide LL-37 was taken up into U937 cells through a distinct endocytic pathway that involved lipid rafts but not macropinosome formation. Although the lipid raft dependence was in line with the reported uptake inhibition of LL-37-DNA complexes into Chinese hamster ovary cells by membrane cholesterol-depleting drugs (60), a reduction in LL-37 uptake in the presence of nocodazole and cytochalasin D was at variance with published studies using A549 epithelial cells (43). These observations point to cell-specific modulation of the uptake process, a circumstance widely documented in the literature (61).

An issue was raised when comparing the flow cytometry data with microscopic observations of intracellular Bac7(1–35) as concerning the cytoplasmic peptide distribution. The appearance of the fluorescein signal was both vesicular and diffuse, in apparent contrast with macropinocytosis being the only uptake mechanism for Bac7(1–35). The diffuse pattern was reminiscent of cationic cell penetrating peptides that enter cells in an endocytosis-independent manner (62). This observation prompted us to consider the additional contribution of direct translocation across the plasma membrane. This view was consistent with the ability of AMPs to target lipid membranes (3, 35, 36) and with the recently published work describing the concurrence of endocytic and membrane-transducing mechanisms in the cellular uptake of a dermaseptin S4 derivative (62) and of oligoarginine peptides (63).

We addressed the membrane transduction issue by analyzing the behavior of Bac7(1–35) on model PC/cholesterol membranes that mimic the zwitterionic membranes of eukaryotic cells, and we showed that Bac7(1–35), but not Bac7(5–35), inserted deeply into the lipid core of these membranes. This behavior correlated with higher membrane affinity and higher insertion constant of Bac7(1–35) compared with Bac7(5–35), as determined by SPR analysis of the binding/insertion process. Taken together, these results indicate the potential for Bac7(1–35) to move across cellular membranes. This conclusion is consistent with both the diffuse cytoplasmic appearance of Bac7(1–35) and with flow cytometry data, indicating incomplete uptake suppression by endocytosis-inhibiting drugs.

Given the capability of Bac7(1–35) to enter mammalian cells without associated toxicity, it seemed reasonable to explore the biological effects of this peptide in connection with its cell interaction properties. We focused on the mitogenic potential on fibroblasts, because fibroblast proliferation and migration are important steps in the tissue repair process. We showed here that Bac7(1–35) induces DNA synthesis in these cells. This is a novel and relevant result providing further evidence of the multifunctional nature of AMPs. Yet a deeper understanding of this activity is required. This issue will be addressed in studies aimed to identify the precise mechanism and the molecular targets of Bac7(1–35). The incapability of Bac7(5–35) to enter 3T3 cells and to affect S phase entry, as observed in the current study, may give useful hints to these studies by suggesting that the immediate targets are intracellular rather than cell surface molecules. It should be noted in this regard that whereas defensins and LL-37 stimulate epithelial cell proliferation through activation of the epidermal growth factor membrane receptor (6), a number of studies of PR-39 have indicated that this peptide may affect a variety of cellular processes through binding to cytoplasmic proteins (12, 14, 15).

In conclusion, the combined results of cell biology-based and model membrane-based experiments performed in this study have increased our understanding of the peptide-cell interactions of cationic peptides by providing insights into the mechanism of internalization of Bac7(1–35), and have extended our knowledge of the biological effects of AMPs on host cells by bringing evidence that Bac7(1–35) stimulates proliferation of fibroblasts.

REFERENCES

1. Levy, O. (2004) *J. Leukocyte Biol.* **76,** 909–925
2. Ganz, T. (2003) *Nat. Rev. Immunol.* **3,** 710–720
3. Oren, Z., and Shai, Y. (1998) *Biopolymers* **47,** 451–463
4. Zanetti, M., Gennaro, R., Skerlavaj, B., Tomasinsig, L., and Circo, R. (2002) *Curr. Pharm. Des.* **8,** 779–793
5. Zanetti, M. (2004) *J. Leukocyte Biol.* **75,** 39–48
6. van Wetering, S., Tjabringa, G. S., and Hiemstra, P. S. (2005) *J. Leukocyte Biol.* **77,** 444–450
7. De, Y., Chen, Q., Schmidt, A. P., Anderson, G. M., Wang, J. M., Wooters, J., Oppenheim, J. J., and Chertov, O. (2000) *J. Exp. Med.* **192,** 1069–1074

8. Chan, Y. R., and Gallo, R. L. (1998) *J. Biol. Chem.* **273,** 28978–28985
9. Gao, Y., Lecker, S., Post, M. J., Hietaranta, A. J., Li, J., Volk, R., Li, M., Sato, K., Saluja, A. K., Steer, M. L., Goldberg, A. L., and Simons, M. (2000) *J. Clin. Investig.* **106,** 439–448
10. Shi, J., Ross, C. R., Leto, T. L., and Blecha, F. (1996) *Proc. Natl. Acad. Sci. U. S. A.* **93,** 6014–6018
11. Gennaro, R., Zanetti, M., Benincasa, M., Podda, E., and Miani, M. (2002) *Curr. Pharm. Des.* **8,** 763–778
12. Gallo, R. L., Ono, M., Povsic, T., Page, C., Eriksson, E., Klagsbrun, M., and Bernfield, M. (1994) *Proc. Natl. Acad. Sci. U. S. A.* **91,** 11035–11039
13. Huang, H. J., Ross, C. R., and Blecha, F. (1997) *J. Leukocyte Biol.* **61,** 624–629
14. Li, J., Post, M., Volk, R., Gao, Y., Li, M., Metais, C., Sato, K., Tsai, J., Aird, W., Rosenberg, R. D., Hampton, T. G., Sellke, F., Carmeliet, P., and Simons, M. (2000) *Nat. Med.* **6,** 49–55
15. Wu, J., Parungo, C., Wu, G., Kang, P. M., Laham, R. J., Sellke, F. W., Simons, M., and Li, J. (2004) *Circulation* **109,** 1660–1667
16. Benincasa, M., Scocchi, M., Podda, E., Skerlavaj, B., Dolzani, L., and Gennaro, R. (2004) *Peptides* (*N. Y.*) **25,** 2055–2061
17. Tomasinsig, L., Scocchi, M., Mettulio, R., and Zanetti, M. (2004) *Antimicrob. Agents Chemother.* **48,** 3260–3267
18. Ghiselli, R., Giacometti, A., Cirioni, O., Circo, R., Mocchegiani, F., Skerlavaj, B., D'Amato, G., Scalise, G., Zanetti, M., and Saba, V. (2003) *Shock* **19,** 577–581
19. Giacometti, A., Cirioni, O., Del Prete, M. S., Skerlavaj, B., Circo, R., Zanetti, M., and Scalise, G. (2003) *J. Antimicrob. Chemother.* **51,** 843–847
20. Rapaport, D., and Shai, Y. (1992) *J. Biol. Chem.* **267,** 6502–6509
21. Kaiser, E., Colescott, R. L., Bossinger, C. D., and Cook, P. I. (1970) *Anal. Biochem.* **34,** 595–598
22. Skerlavaj, B., Romeo, D., and Gennaro, R. (1990) *Infect. Immun.* **58,** 3724–3730
23. Goruppi, S., Ruaro, E., Varnum, B., and Schneider, C. (1997) *Mol. Cell. Biol.* **17,** 4442–4453
24. Leclerc, M., Cosson, G., and Vagner, D. (1967) *Ann. Biol. Clin.* (*Paris*) **25,** 469–474
25. Gazit, E., Lee, W. J., Brey, P. T., and Shai, Y. (1994) *Biochemistry* **33,** 10681–10692
26. Sims, P. J., Waggoner, A. S., Wang, C. H., and Hoffmann, J. R. (1974) *Biochemistry* **13,** 3315–3330
27. Loew, L. M., Rosenberg, I., Bridge, M., and Gitler, C. (1983) *Biochemistry* **22,** 837–844
28. Shai, Y., Bach, D., and Yanovsky, A. (1990) *J. Biol. Chem.* **265,** 20202–20209
29. Oren, Z., and Shai, Y. (2000) *Biochemistry* **39,** 6103–6114
30. Surewicz, W. K., Mantsch, H. H., and Chapman, D. (1993) *Biochemistry* **32,** 389–394
31. Harrick, N. J. (1967) *Internal Reflection Spectroscopy*, Interscience, New York
32. Ishiguro, R., Kimura, N., and Takahashi, S. (1993) *Biochemistry* **32,** 9792–9797
33. Mozsolits, H., Wirth, H. J., Werkmeister, J., and Aguilar, M. I. (2001) *Biochim. Biophys. Acta* **1512,** 64–76
34. Morton, T. A., Myszka, D. G., and Chaiken, I. M. (1995) *Anal. Biochem.* **227,** 176–185
35. Oren, Z., Lerman, J. C., Gudmundsson, G. H., Agerberth, B., and Shai, Y. (1999) *Biochem. J.* **341,** 501–513
36. Johansson, J., Gudmundsson, G. H., Rottenberg, M. E., Berndt, K. D., and Agerberth, B. (1998) *J. Biol. Chem.* **273,** 3718–3724
37. Turner, J., Cho, Y., Dinh, N. N., Waring, A. J., and Lehrer, R. I. (1998) *Antimicrob. Agents Chemother.* **42,** 2206–2214
38. Richard, J. P., Melikov, K., Vives, E., Ramos, C., Verbeure, B., Gait, M. J., Chernomordik, L. V., and Lebleu, B. (2003) *J. Biol. Chem.* **278,** 585–590
39. Wadia, J. S., Stan, R. V., and Dowdy, S. F. (2004) *Nat. Med.* **10,** 310–315
40. West, M. A., Bretscher, M. S., and Watts, C. (1989) *J. Cell Biol.* **109,** 2731–2739
41. Muro, S., Wiewrodt, R., Thomas, A., Koniaris, L., Albelda, S. M., Muzykantov, V. R., and Koval, M. (2003) *J. Cell Sci.* **116,** 1599–1609
42. Conner, S. D., and Schmid, S. L. (2003) *Nature* **422,** 37–44
43. Lau, Y. E., Rozek, A., Scott, M. G., Goosney, D. L., Davidson, D. J., and Hancock, R. E. (2005) *Infect. Immun.* **73,** 583–591
44. Oren, Z., and Shai, Y. (1996) *Biochemistry* **36,** 1826–1835
45. Byler, D. M., and Susi, H. (1986) *Biopolymers* **25,** 469–487
46. Jackson, M., and Mantsch, H. H. (1995) *Crit. Rev. Biochem. Mol. Biol.* **30,** 95–120
47. Frey, S., and Tamm, L. K. (1991) *Biophys. J.* **60,** 922–930
48. Pezolet, M., Bonenfant, S., Dousseau, F., and Popineau, Y. (1992) *FEBS Lett.* **299,** 247–250
49. Oren, Z., Hong, J., and Shai, Y. (1999) *Eur. J. Biochem.* **259,** 360–369
50. Hong, J., Oren, Z., and Shai, Y. (1999) *Biochemistry* **38,** 16963–16973
51. Sharon, M., Oren, Z., Shai, Y., and Anglister, J. (1999) *Biochemistry* **38,** 15305–15316
52. Papo, N., Oren, Z., Pag, U., Sahl, H. G., and Shai, Y. (2002) *J. Biol. Chem.* **277,** 33913–33921
53. Tatulian, S. A., Biltonen, R. L., and Tamm, L. K. (1997) *J. Mol. Biol.* **268,** 809–815
54. Cameron, D. G., Casal, H. L., Gudgin, E. F., and Mantsch, H. H. (1980) *Biochim. Biophys. Acta* **596,** 463–467
55. Papo, N., and Shai, Y. (2004) *Biochemistry* **43,** 6393–6403
56. Bowdish, D. M., Davidson, D. J., and Hancock, R. E. (2005) *Curr. Protein Pept. Sci.* **6,** 35–51
57. Drin, G., Cottin, S., Blanc, E., Rees, A. R., and Temsamani, J. (2003) *J. Biol. Chem.* **278,** 31192–31201
58. Kobayashi, S., Chikushi, A., Tougu, S., Imura, Y., Nishida, M., Yano, Y., and Matsuzaki, K. (2004) *Biochemistry* **43,** 15610–15616
59. Sadler, K., Eom, K. D., Yang, J. L., Dimitrova, Y., and Tam, J. P. (2002) *Biochemistry* **41,** 14150–14157
60. Sandgren, S., Wittrup, A., Cheng, F., Jonsson, M., Eklund, E., Busch, S., and Belting, M. (2004) *J. Biol. Chem.* **279,** 17951–17956
61. Le, P. U., and Nabi, I. R. (2003) *J. Cell Sci.* **116,** 1059–1071
62. Mano, M., Teodosio, C., Paiva, A., Simoes, S., and Pedroso de Lima, M. C. (2005) *Biochem. J.* **390,** 603–612
63. Zaro, J. L., and Shen, W. C. (2005) *Exp. Cell Res.* **307,** 164–173